AMERICAN SOCIETY FOR MICROBIOLOGY | Molecular and Cellular Biology®

RESEARCH ARTICLE

The Chromatin-Associated Phf12 Protein Maintains Nucleolar Integrity and Prevents Premature Cellular Senescence

Richard Graveline,[a] Katarzyna Marcinkiewicz,[a] Seyun Choi,[a] Marilène Paquet,[b] Wolfgang Wurst,[c] Thomas Floss,[c] Gregory David[a]

New York University School of Medicine, New York, New York, USA[a]; Faculté de Médecine Vétérinaire, Université de Montréal, Saint-Hyacinthe, Québec, Canada[b]; Helmholtz Zentrum München-German Research Center for Environmental Health, Neuherberg, Germany[c]

ABSTRACT Pf1, also known as Phf12 (plant homeodomain [PHD] zinc finger protein 12), is a member of the PHD zinc finger family of proteins. Pf1 associates with a chromatin-interacting protein complex comprised of MRG15, Sin3B, and histone deacetylase 1 (HDAC1) that functions as a transcriptional modulator. The biological function of Pf1 remains largely elusive. We undertook the generation of *Pf1* knockout mice to elucidate its physiological role. We demonstrate that *Pf1* is required for mid- to late gestation viability. *Pf1* inactivation impairs the proliferative potential of mouse embryonic fibroblasts (MEFs) and is associated with a significant decrease in bromodeoxyuridine incorporation; an increase in senescence-associated β-galactosidase (SA-β-Gal) activity, a marker of cellular senescence; and elevated levels of phosphorylated H2AX (γ-H2A.X), a marker associated with DNA double-strand breaks. Analysis of transcripts differentially expressed in wild-type and Pf1-deficient cells revealed the impact of Pf1 in multiple regulatory arms of the ribosome biogenesis pathways. Strikingly, assessment of the morphology of the nucleoli exposed an abnormal nucleolar structure in Pf1-deficient cells. Finally, proteomic analysis of the Pf1-interacting complexes highlighted proteins involved in ribosome biogenesis. Taken together, our data reveal an unsuspected function for the Pf1-associated chromatin complex in the ribosomal biogenesis and senescence pathways.

KEYWORDS transcription, ribosome, Pf1, senescence, nucleolus

Received 23 September 2016 **Returned for modification** 9 November 2016 **Accepted** 4 December 2016

Accepted manuscript posted online 12 December 2016

Citation Graveline R, Marcinkiewicz K, Choi S, Paquet M, Wurst W, Floss T, David G. 2017. The chromatin-associated Phf12 protein maintains nucleolar integrity and prevents premature cellular senescence. Mol Cell Biol 37:e00522-16. https://doi.org/10.1128/MCB.00522-16.

Address correspondence to Gregory David, gregory.david@nyumc.org.

R.G. and K.M. contributed equally to this article.

Pf1, also known as Phf12 (plant homeodomain [PHD] zinc finger protein 12), is a member of the PHD zinc finger family of proteins. PHD domains are small, 50- to 80-amino-acid-long domains often found in clusters of two or three and/or in the proximity of other chromatin-interacting domains, such as bromo- or chromodomains. Consistently, many of the PHD-containing proteins are nuclear proteins that interact with chromatin. Increasing evidence suggests that PHD domains are capable of recognizing modified and unmodified histone tails and that PHD domain-containing proteins act as epigenetic readers (1).

The *Pf1* gene is conserved throughout evolution, and the Pf1 protein, like its *Saccharomyces cerevisiae* yeast homolog, Rco1, contains two PHD domains in its N terminus. Mammalian Pf1 was first identified in a yeast two-hybrid screen for proteins interacting with the paired amphipathic helix 2 (PAH2) domain of Sin3A and shown to function as a transcriptional repressor (2). A later report identified Pf1 to be one of the components of the human MRG15 complex, together with Sin3B but not together with its close homolog, Sin3A (3). The PHD domains of Pf1 are important for the interaction with the MRG domain of MRG15, which relies mainly on hydrophobic interactions (3–5). The interaction of Pf1 with a complex containing Sin3B but not Sin3A was also confirmed in experiments identifying associations between Sin3B, histone deacetylase

1 (HDAC1), MRG15, and Pf1. While its precise function in transcriptional regulation remains unclear, the Pf1-MRG15-Sin3B-HDAC complex appears to modulate RNA polymerase II (RNAPII) progression at actively transcribed regions, similar to what has been reported for the Rpd3S complex, its yeast homolog (6).

Reports assessing the biological function of Pf1 point to roles in phosphoinositide signaling (7), nervous system development (8), and the epithelial-to-mesenchymal transition and maintenance of a stem cell phenotype (9). To our knowledge, no comprehensive study elucidating the *in vivo* function of the Pf1 protein has been conducted so far.

Mouse strains with genetic inactivation of Sin3B, HDAC1, or MRG15, the three components of the protein complex repeatedly shown to also contain the Pf1 protein, have previously been described. Sin3B$^{-/-}$ embryos reveal a global retardation in size, a pale color, an abnormal hematopoietic picture in the liver, and a reduction in bone deposition at later embryonic stages and die shortly before birth (10). Sin3B knockout mouse embryonic fibroblasts (MEFs) are refractory to quiescence and to oncogene-induced senescence (OIS), a stable cell cycle arrest in response to oncogene activation (10–13). Knockout of HDAC1 leads to embryonic lethality before day 10.5 of gestation, and HDAC1$^{-/-}$ embryos examined at earlier embryonic stages are extremely growth retarded as a result of a defect in cell proliferation (14, 15). The loss of HDAC1 in embryonic stem (ES) cells leads to impaired proliferation that is associated with upregulated expression of cyclin-dependent kinase inhibitors p21 and p27 (14), but conditional HDAC1 knockout in MEFs does not affect cell proliferation under normal conditions (16). Similarly, genetic inactivation of MRG15 results in embryonic lethality between embryonic day 14.5 (E14.5) and birth. The null embryos are smaller than the wild-type (wt) and heterozygous embryos, with the most prominent defects being seen in the heart, lung, liver, and keratinocyte-epidermal layer of the skin. The growth potential of Mrg15$^{-/-}$ MEFs is greatly reduced (17).

Here, we describe the generation of *Pf1* knockout mice to define the physiological role of Pf1. We report that *Pf1* inactivation leads to embryonic lethality. Moreover, we show that *Pf1* inactivation impairs the proliferative potential of the cells and is associated with a strong nucleolar stress. Taken together, our data demonstrate that Pf1 is crucial for embryogenesis and nuclear functions.

RESULTS

Pf1 is required for proper mid- to late gestation development. To investigate the biological functions of Pf1 in a physiologically relevant system, we generated a mouse strain harboring a genetic inactivation of the *Pf1* locus. Specifically, we identified a mouse ES cell clone harboring a retroviral insertion in the 5′ region of *Pf1*, which results in the disruption of a splice acceptor site (Fig. 1A). We then used this ES cell clone to derive a Pf1$^{+/-}$ mouse strain. Germ line transmission of the mutant *Pf1* allele was verified by PCR, and heterozygous mice were intercrossed to obtain Pf1$^{-/-}$ embryos (Fig. 1B). Genetic inactivation of *Pf1* in the Pf1$^{-/-}$ embryos was verified by quantitative reverse transcriptase PCR (qRT-PCR) (Fig. 1C), and embryonic development was followed. While *Pf1* heterozygous mice developed normally, no live Pf1$^{-/-}$ mouse was born. Temporal analysis of embryonic development revealed that Pf1$^{-/-}$ embryos die at mid- to late gestation with diverse developmental defects, including edema and internal hemorrhage (Fig. 1D and E). Moreover, macroscopic analysis of the Pf1$^{-/-}$ embryos indicated a global growth retardation, where E14.5 Pf1$^{-/-}$ embryos were comparable in size to E11.5 wild-type embryos (Fig. 1F and data not shown). Pf1$^{-/-}$ embryos also presented impaired development of the skeleton, of the associated skeletal muscle, and of the brain (Fig. 1F). To determine if the global growth retardation observed at stage E14.5 results from a decrease in cell proliferation or, alternatively, from an increase in cell apoptosis, we performed immunohistological staining on the whole embryo at stage E14.5 for Ki67, a cell proliferation marker, and caspase-3 (Casp3), an effector caspase and a marker of the cell commitment to apoptosis. No difference in the levels of Ki67 was observed at this stage (Fig. 1G). In contrast, a localized increase

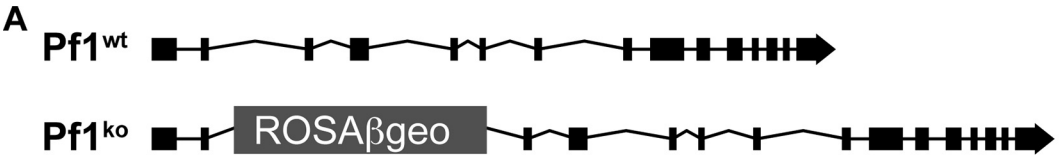

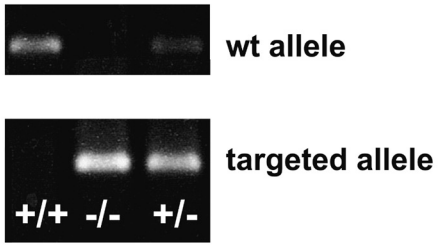

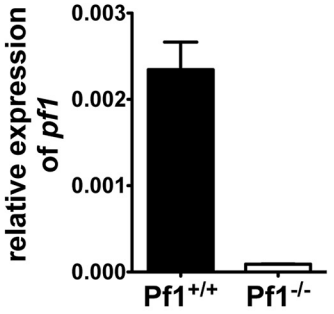

D

Stage	Pf1$^{+/+}$ No.	(%)	Pf1$^{+/-}$ No.	(%)	Pf1$^{-/-}$ No.	(%)	Total
E12.5	4	(40.0)	4	(40.0)	2	(20.0)	10
E13.5	7	(30.4)	10	(43.5)	6	(26.1)	23
E14.5	9	(20.9)	27	(62.8)	7	(16.3)	43
E18.5	10	(38.5)	16	(61.5)	-	(00.0)	26
Day 14	11	(32.4)	23	(67.6)	-	(00.0)	34

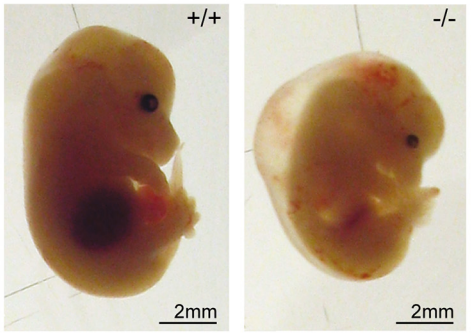

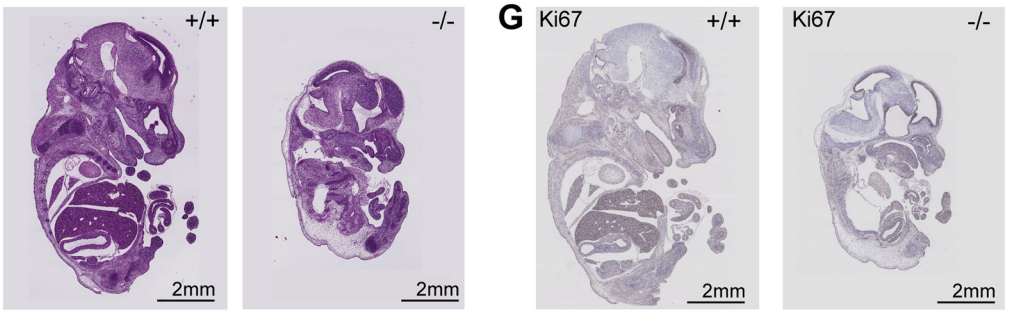

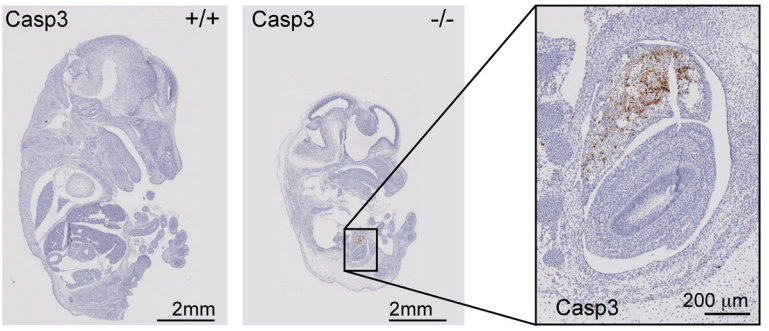

FIG 1 Pf1 is required for proper mid- to late gestation development (A) Schematic representation of the wild-type (top) or mutated (knockout [ko]; bottom) allele for *Pf1*. (B) Endpoint genotyping PCR for *Pf1* of embryos of the indicated genotype obtained at day 14.5 postcoitus. (C) qRT-PCR for expression of *Pf1* in Pf1$^{+/+}$ and Pf1$^{-/-}$ embryos. (D) Genotype distribution of embryos from Pf1 heterozygote intercrosses in a C57BL/6 mouse background (E, embryonic day). The number of animals analyzed per genotype and time point is indicated, and the corresponding percentage is provided in parentheses. (E) Representative pictures of Pf1$^{+/+}$ and Pf1$^{-/-}$ embryos at E14.5. (F) Hematoxylin- and eosin-stained sections of whole Pf1$^{+/+}$ and Pf1$^{-/-}$ embryos. (G) Immunohistochemistry staining for Ki67 in Pf1$^{+/+}$ and Pf1$^{-/-}$ embryos obtained on day 14.5 postcoitus. (H) Immunohistochemistry staining for Casp3 in Pf1$^{+/+}$ and Pf1$^{-/-}$ embryos obtained on day 14.5 postcoitus. (Right) Magnification of the liver of Pf1$^{-/-}$ embryos.

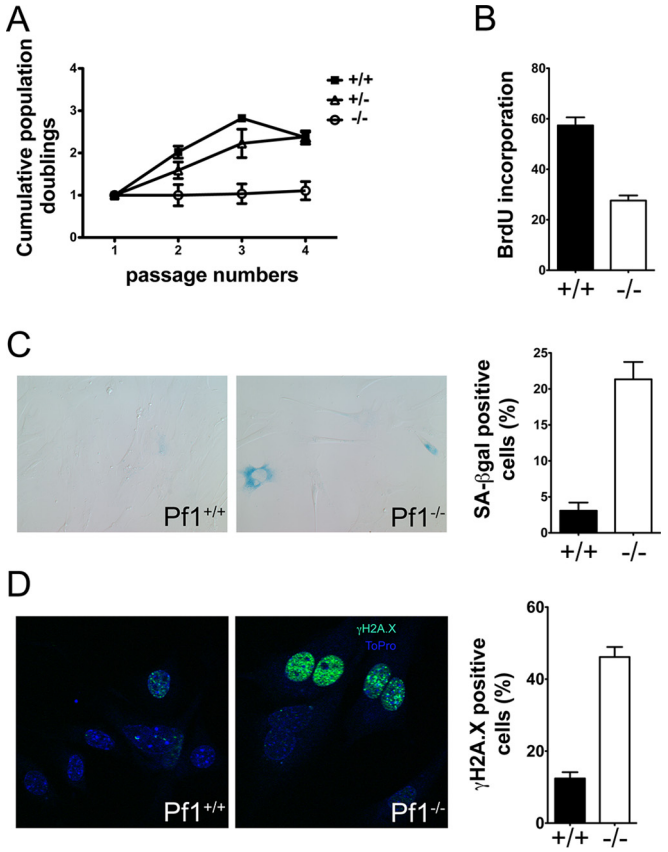

FIG 2 Pf1 prevents premature entry into replicative senescence. (A) Growth curves using a 3T3 protocol on early-passage Pf1$^{+/+}$, Pf1$^{+/-}$, and Pf1$^{-/-}$ embryos. (B) BrdU incorporation after a 2-h pulse of 20 μM BrdU by Pf1$^{+/+}$ and Pf1$^{-/-}$ early-passage primary MEFs. For each condition, at least 200 cells were counted ($n = 3$). (C) Quantification of SA-β-Gal-positive cells in Pf1$^{+/+}$ and Pf1$^{-/-}$ early-passage primary MEFs. (Left two panels) Representative pictures of SA-β-Gal staining for the Pf1$^{+/+}$ and Pf1$^{-/-}$ genotypes; (right) percentage of SA-β-Gal-positive cells after counting at least 200 cells ($n = 3$). (D) γ-H2A.X immunofluorescence staining for Pf1$^{+/+}$ and Pf1$^{-/-}$ early-passage primary MEFs. (Left two panels) Representative pictures of γ-H2AX-positive Pf1$^{+/+}$ and Pf1$^{-/-}$ MEFs; (right) percentage of γ-H2AX-positive cells after counting at least 200 cells ($n = 3$).

in Casp3 levels was observed in the livers of Pf1$^{-/-}$ embryos (Fig. 1H). Overall, these observations indicate that Pf1 is essential for normal embryonic development and Pf1 protects from aberrant apoptosis in a tissue-specific manner.

Pf1 prevents premature entry into replicative senescence. We next generated mouse embryonic fibroblasts (MEFs) from E14.5 Pf1$^{+/+}$, Pf1$^{+/-}$, and Pf1$^{-/-}$ embryos to assess the cellular function of Pf1. Following a standard 3T3 protocol, we observed no significant differences in the ability of Pf1$^{+/+}$ and Pf1$^{+/-}$ MEFs to proliferate (Fig. 2A). In contrast, Pf1$^{-/-}$ MEFs lost their proliferative capacity as early as during the first cell passage. This result suggests that Pf1 functions to maintain a cellular proliferative state under culture conditions. The decreased proliferative potential of Pf1$^{-/-}$ MEFs was associated with a significant decrease in bromodeoxyuridine (BrdU) incorporation and an increase in senescence-associated β-galactosidase (SA-β-Gal) activity, a marker of cellular senescence (Fig. 2B and C, respectively). Cellular senescence can be triggered by the accumulation of irreparable DNA damage (18). Thus, we assessed the levels of phosphorylated H2AX (γ-H2A.X), a marker associated with DNA double-strand breaks, in Pf1$^{-/-}$ and Pf1$^{+/+}$ MEFs. Consistent with the increased senescence detected in Pf1-null cells, Pf1$^{-/-}$ cells exhibited a strong activation of the DNA damage response, as visualized by an increase in the γ-H2AX signal compared to that for control cells (Fig. 2D). Thus, our results suggest that Pf1 is essential to prevent premature cell cycle exit and entry into cellular senescence.

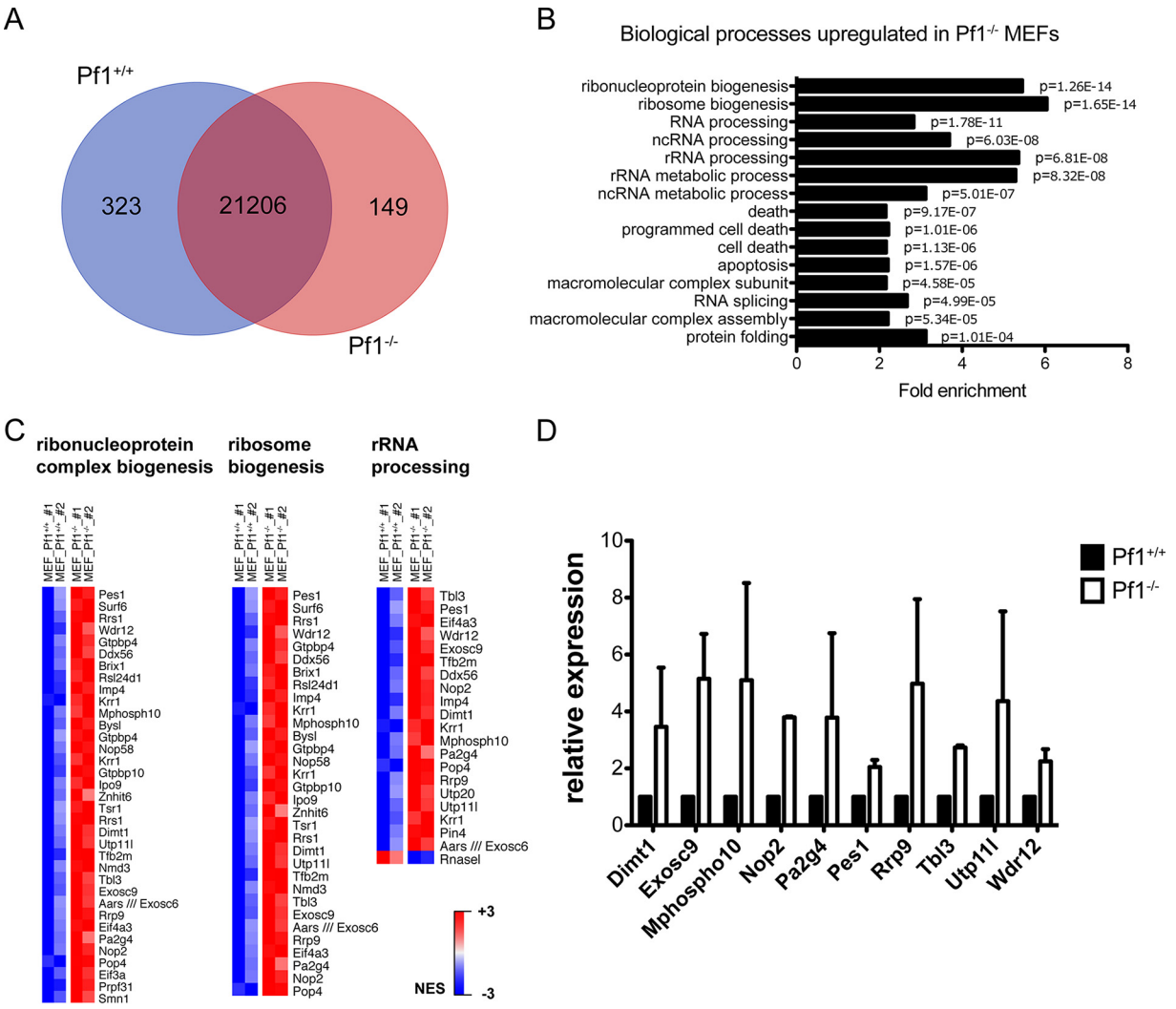

FIG 3 Pf1 is involved in maintaining the equilibrium of the rRNA processing pathway (A) Venn diagram representation of differential gene expression in Pf1$^{+/+}$ and Pf1$^{-/-}$ early-passage primary MEFs. (B) Pathway enrichment analysis using gene ontology analysis with DAVID of genes transcriptionally induced upon Pf1 deletion in MEFs. GO analyses were performed with genes that presented at least a 2-fold significant change in expression in Pf1$^{-/-}$ early-passage primary MEFs compared to Pf1$^{+/+}$ early-passage primary MEFs ($P < 0.05$). The bars represent the fold enrichment of the pathway in order of significance (*P* values), listed on the right of the bars. Functional categorizations of differentially expressed genes upon knockout of *Pf1* were analyzed by gene ontology biological process (GO_BP). ncRNA, noncoding RNA. (C) Heat map representation of enriched expression for ribonucleoprotein complex biogenesis, ribosome biogenesis, and rRNA processing pathways in Pf1$^{+/+}$ and Pf1$^{-/-}$ MEFs. The heat map represents the top enriched genes in Pf1$^{-/-}$ MEFs compared to Pf1$^{+/+}$ MEFs. NES, normalized enrichment score (red, high levels of expression; blue, low levels of expression). (D) Results of qRT-PCR for a subset of genes present in the ribonucleoprotein complex biogenesis, ribosome biogenesis, and rRNA processing pathways. The Pf1$^{-/-}$ mRNA expression levels are relative to the Pf1$^{+/+}$ mRNA expression levels ($n = 3$).

Pf1 is involved in maintaining the equilibrium of the rRNA processing pathway. To identify the molecular mechanisms underlying the defects elicited by genetic inactivation of *Pf1*, we next examined the impact of *Pf1* inactivation on the MEF transcriptome. RNA extracted from wild-type and Pf1-null MEFs was profiled by hybridization to a whole-genome microarray. As shown in Fig. 3A, Pf1 depletion led to specific changes in gene expression, with 149 genes being upregulated and 323 genes being downregulated by a 2-fold change ($P < 0.05$) in Pf1$^{-/-}$ MEFs. Gene ontology (GO) analysis by analysis of the transcripts differentially expressed in wild-type and Pf1-deficient cells with the Database for Annotation, Visualization, and Integrated Discovery (DAVID) revealed the impact of Pf1 in multiple regulatory arms of the RNA biogenesis and maturation pathways (Fig. 3B). Specifically, genetic inactivation of Pf1 resulted in a strong and significant increase in the abundance of a large number of transcripts involved in

ribosome biogenesis and rRNA processing (Fig. 3B and C). This finding was further validated by qRT-PCR for a subset of genes, including the genes for Dimt1 (dimethyladenosine transferase 1 homolog, an rRNA methyltransferase), Pes1 (pescadillo ribosomal biogenesis factor 1, a component of PeBoW complex with roles in pre-rRNA processing and 60S ribosomal subunit maturation), and Pa2G4 (proliferation-associated 2G4, involved in ribosome assembly and the regulation of intermediate and late steps of rRNA processing) (Fig. 3D). Thus, our results suggest that Pf1 plays an important role in regulating the levels of transcripts involved in ribosomal biosynthesis and rRNA processing.

Pf1$^{-/-}$ MEFs undergo changes in nucleolar structure. The nucleolus is the site of rRNA synthesis and nascent ribosome assembly (19). Previous studies pointed to a link between nucleolar stress and cellular senescence (20, 21), although the molecular bases for this link remain elusive. To confirm our observations that Pf1 deletion affects expression of the rRNA processing machinery, we analyzed by immunofluorescence the levels of fibrillarin, SENP3, and UBF, three integral components of the nucleolus that participate in rRNA processing. Fibrillarin is an rRNA 2′-*O*-methyltransferase involved in the early stages of rRNA processing (22–25). SENP3 is a SUMO-isopeptidase involved in the conversion of the 32S rRNA intermediate to mature 28S rRNA in mammals (26–28). SENP3 also tightly associates with the nucleophosmin NPM1, another central factor in ribosome biogenesis (29, 30). Fibrillarin and SENP3 exert their function and are present in the outer two layers of the nucleoli: the dense fibrillar component and the granular component. UBF is essential for RNA polymerase I (Pol I) preinitiation complex binding to enhancer regions of ribosomal DNA (rDNA) sequences; it exerts its functions in the fibrillar center of the nucleolus and also contributes to rRNA processing (22). As shown in Fig. 4, genetic inactivation of Pf1 alters the shape and size of the nucleolus. Indeed, the nucleolus of the wild-type Pf1 MEFs visualized by fibrillarin and SENP3 immunofluorescence appears as multiple small units (Fig. 4A and B). The staining pattern for these markers was strikingly different in Pf1$^{-/-}$ MEFs, with an increase in the fluorescence intensity and a denser distribution in fewer spots being seen within the nucleus, indicating a reorganization of the nucleolus in these cells. However, disruption of the nucleolar structure was not generalized since no difference in the intensity or distribution of the UBF signal was observed between Pf1$^{+/+}$ and Pf1$^{-/-}$ MEFs (Fig. 4C). This result suggests that Pf1 controls the expression of specific components of the rRNA processing machinery and affects the outer nucleolar structure.

Proteomic characterization of Pf1-interacting factors identifies interactions with proteins involved in ribosomal biogenesis. To identify the molecular basis underlying the impact of Pf1 on nucleolar structure and function, we aimed to identify novel Pf1-interacting proteins. To do so, we generated Flag-tagged constructs of wild-type Pf1 and two Pf1 variants with point mutations unable to interact either with MRG15 or with histone H3 (the Pf1^{F210A} and Pf1^{D57N} mutants, respectively [5, 31]). We then stably expressed the three constructs in HeLa S3 cells, extracted nuclear proteins, immunoprecipitated protein complexes containing the Pf1 construct using anti-Flag beads, and analyzed the protein composition of the precipitated complexes by liquid chromatography-tandem mass spectrometry (LC-MS/MS). Silver-stained electrophoresis gels of the precipitated proteins revealed a discrete band at about 130 kDa, which corresponds to the apparent molecular mass of Pf1, that was present in Pf1, Pf1^{F210A}, and Pf1^{D57N} samples but absent in the control HeLa cell lysate infected with the pBabe empty vector (Fig. 5A). Moreover, a second prominent band at about 38 kDa, which corresponds to the apparent molecular mass of MRG15, was observed only for wild-type Pf1 and the Pf1^{D57N} mutant but not the Pf1^{F210A} mutant, as expected (Fig. 5A). The precipitated proteins were then analyzed by nano-LC-MS/MS to identify the Pf1-associated proteins. As shown in Table 1, this analysis identified most of the proteins previously known to be components of the mammalian homolog of the Rpd3S complex and, to a lesser extent, of the canonical Sin3-HDAC complex. Notably, the enrichment confirmed the interaction between Pf1 and the histone H3 lysine 4 (H3K4)-specific demethylase KDM5A, EMSY, GATAD1, Sin3B, HDAC1, and MRG15 (5, 6). Thus,

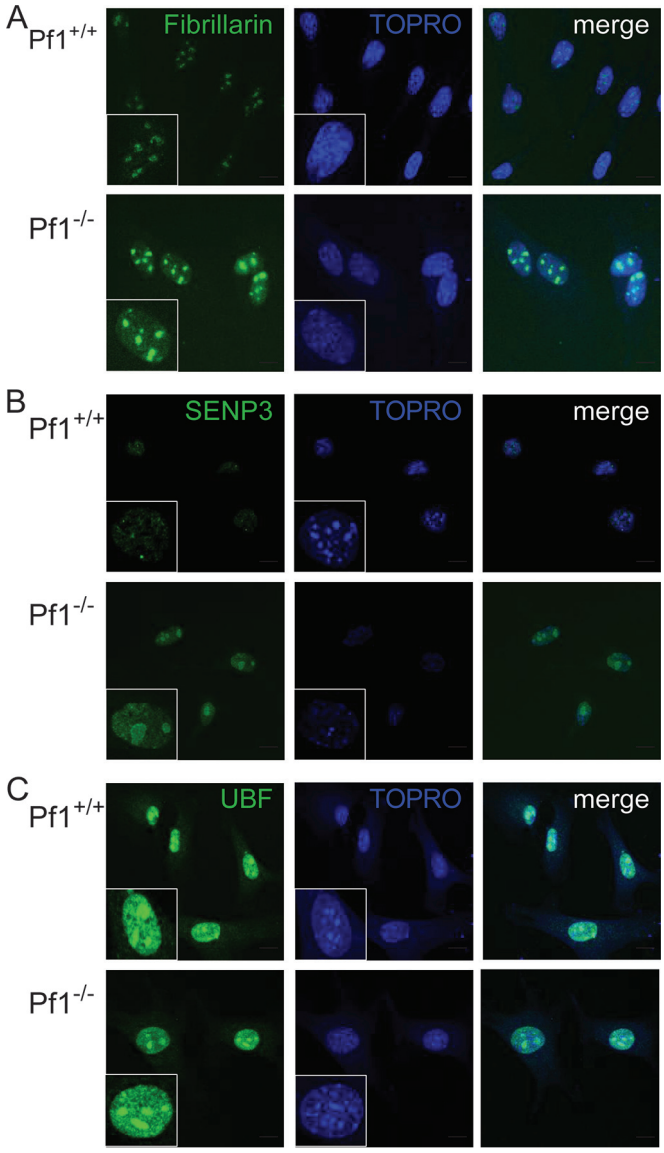

FIG 4 Pf1 inactivation is associated with morphological changes in the nucleolus. Representative immunofluorescence staining on $Pf1^{+/+}$ and $Pf1^{-/-}$ MEFs for fibrillarin (A), SENP3 (B), and UBF (C).

this result further confirmed a physical basis for the functional involvement of Pf1 in transcriptional regulation and the stable association between Pf1, Sin3B, and a discrete group of proteins previously known to be the components of the mammalian homolog of the Rpd3S complex (3, 6, 32, 33).

Our analysis also points to the requirement of a Pf1 association with MRG15 for Pf1 interaction with some proteins, including components of the canonical Sin3-HDAC complex. Indeed, Table 2 lists the proteins that we identified to be Pf1 interactors dependent upon the Pf1 association with either MRG15 or histone H3 (proteins coimmunoprecipitated with the wt Pf1 construct but not with the mutant $Pf1^{F210A}$ or $Pf1^{D57N}$ construct, respectively). Consistent with its known function in transcriptional regulation, the proteins most abundantly coimmunoprecipitated with wt Pf1 are involved in chromosome and chromatin organization, protein complex biogenesis, transcription, cell cycle control, and nuclear transport (Table 3). Importantly, LC-MS/MS analysis also revealed the association of Pf1 with several proteins not previously identified to interact with Pf1. Table 4 lists some of these newly found possible Pf1 interactors, grouped according to the biological process annotations. Interestingly,

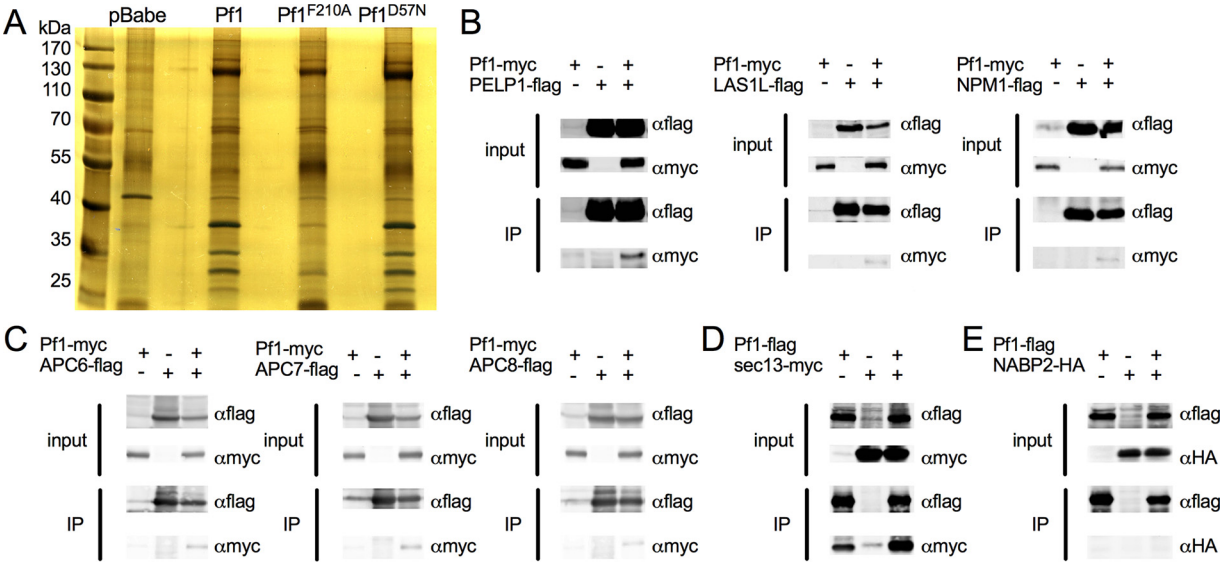

FIG 5 Pf1 interaction network. (A) Pf1-associated proteins immunopurified from a HeLa S3 cell nuclear extract (NE) stably expressing a Flag-tagged version of wt Pf1 or versions of Pf1 with point mutations ($Pf1^{F210A}$ and $Pf1^{D57N}$). Proteins were resolved by SDS-PAGE and revealed by silver staining. (B to D) Coimmunoprecipitation analysis to confirm the association of Pf1 with selected proteins involved in the ribosome biogenesis pathway (B) and components of the anaphase-promoting complex (C) and nucleopore complex (D). (E) Negative control for the coimmunoprecipitation experiments. IP, immunoprecipitation; HA, hemagglutinin.

LC-MS/MS analysis of Pf1-associated complexes highlighted proteins with roles in ribosome biogenesis, similar to the gene ontology terms associated with transcripts expressed at higher levels in Pf1 knockout MEFs than wt Pf1 MEFs (Fig. 3B). These proteins identified by LC-MS/MS include ribosomal biogenesis protein LAS1L (LAS1L); nucleolar proteins 56 and 58 (NOP56 and NOP58, respectively); proline-, glutamic acid-, and leucine-rich protein 1 (PELP1); nucleophosmin 1 (NPM1); fibrillarin (FBL); testis expressed 10 (TEX10); WD repeat domain 3 and 18 (WDR3 and WDR18, respectively); BMS1 homolog, ribosome assembly protein (BMS1); as well as ribosomal proteins S6, S7, S14, and S16 (RPS6, RPS7, RPS14, and RPS16, respectively) and other proteins (Table 4). A complex comprising PELP1, TEX10, WDR18, and SENP3 has already been described (27). Additionally, the same report demonstrated that PELP1 and LAS1L are SUMOylated by the SENP3 isopeptidase (27). SENP3 is a marker of the outer two layers of the nucleoli (the dense fibrillar and granular components), and we have shown that anti-SENP3 antibody staining of the nucleoli is more intense in $Pf1^{-/-}$ MEFs than in control cells, marking a few large and clearly visible intranuclear structures in $Pf1^{-/-}$ MEFs, as

TABLE 1 Composition of the main complex associated with Pf1

Description	Score	No. of peptides	Molecular mass (kDa)
Pf1-Sin3B core complex			
GATAD1	63.67	11	28.7
MORF4L2	121.93	18	32.3
KDM5A	329.82	61	192.0
Sin3B	261.28	38	129.3
EMSY	205.31	35	141.4
ZNF131	31.17	7	67.3
MORF4L1	223.52	23	37.2
Sin3A complex			
Sin3A	196.66	37	145.1
SDS3	45.29	77	38.1
SAP30	7.33	2	23.3
SAP130	24.36	7	113.9
HDAC1	114.20	12	55.1
Rbbp7	74.59	11	47.8
Rbbp4	27.46	5	46.1

TABLE 2 Proteins for which the F210A or D57N substitution affects the association with Pf1

Mutant protein(s)	Protein(s) specifically absent in samples from which $Pf1^{F210A}$, $Pf1^{D57N}$, or both were immunoprecipitated
$Pf1^{F210A}$	MORF4L2, APC1, APC7, POLR2B, RANGP1, ZBTB7A
$Pf1^{D57N}$	CDK9
$Pf1^{F210A}$ and $Pf1^{D57N}$	Sin3A, KPNB1, USP7, CCAR2

opposed to more diffuse, multiple small puncta in the wt cells (see above and Fig. 4B). Finally, other examples of newly identified Pf1-associated functional protein clusters include components of the anaphase-promoting complex or proteins involved in transport through the nuclear envelope (Table 4).

We thus conducted coimmunoprecipitation (co-IP) experiments using tagged constructs of Pf1 and selected potential novel Pf1 interaction candidates identified in our LC-MS/MS experiment, as well as an additional component of the anaphase-promoting complex, namely, ACP8. Compared to the results obtained with our negative control, SOSS complex subunit B1 (NABP2) (Fig. 5E), all the co-IPs performed showed a clear interaction between Pf1 and the proteins tested (Fig. 5B to D). The interaction with Pf1 was particularly strong for PELP1 (Fig. 5B) and Sec13 (Fig. 5D). Altogether, these results corroborate the findings of our LC-MS/MS analysis and suggest that Pf1 directly contributes to the maintenance of nucleolar functions through its interaction with proteins that participate in ribosomal biogenesis. Along with the demonstration that Pf1 regulates the transcription of genes involved in the rRNA pathway, our results indicate that Pf1 may coordinate transcriptional and posttranscriptional steps of ribosomal biogenesis.

DISCUSSION

We undertook the generation and characterization of Pf1 knockout mice in order to define the physiological role of Pf1. Pf1 was first identified to be a component of the Sin3-HDAC complex. Specifically, Pf1 appears to interact directly with the Sin3 scaffold

TABLE 3 GO analysis of proteins that associate with Pf1[a]

Biological process term	Fold enrichment	*P* value
Chromosome organization	5.51	1.30E−07
Protein complex biogenesis	5.29	2.19E−07
Protein complex assembly	5.29	2.19E−07
Chromatin organization	6.19	2.98E−07
Transcription	2.54	3.89E−07
Cellular protein complex assembly	10.31	4.54E−07
Chromatin modification	7.31	5.85E−07
Negative regulation of macromolecule metabolic process	4.10	1.03E−06
M phase	6.09	3.49E−06
Response to unfolded protein	16.47	3.73E−06
Cell cycle phase	5.24	5.28E−06
Macromolecular complex assembly	4.02	6.81E−06
DNA metabolic process	4.62	7.64E−06
Protein folding	8.49	9.53E−06
Protein import into nucleus	13.59	1.14E−05
Nuclear import	13.29	1.30E−05
Macromolecular complex subunit organization	3.76	1.49E−05
Protein localization in nucleus	12.44	1.90E−05
Nucleocytoplasmic transport	8.56	3.72E−05
Response to protein stimulus	10.93	3.98E−05
Nuclear transport	8.46	4.04E−05
Histone H2A acetylation	55.67	4.22E−05
Mitosis	6.83	4.57E−05
Nuclear division	6.83	4.57E−05
M phase of mitotic cell cycle	6.71	5.19E−05

[a]Entries were grouped according to their association with the indicated gene ontology biological process terms. The fold enrichment and *P* values shown were obtained using the DAVID functional annotation tool and the list of proteins most abundantly associated with wt Pf1 in our LC-MS/MS analysis.

TABLE 4 Novel proteins found to associate with Pf1[a]

GO accession no., biological process term	Proteins	*P* value
GO|0031145, anaphase-promoting complex-dependent proteasomal ubiquitin-dependent protein catabolic process	APC1, CDK1, APC5, PSMA4, APC4, CDC23, UBC	1.69E−03
GO|0051169, nuclear transport	NCBP1, MCM3AP, NUP160, RAN, IPO5, SPTBN1, NOP58, KPNA4, RANBP2, THOC2, KPNA2, KPNB1, KPNA1	6.65E−05
GO|0042254, ribosome biogenesis	NPM1, LAS1L, NOP58, FBL, RPS2, PELP1, RPS4X, RPS5, RPS3, HEATR1, RPS8, RPS6, GEMIN4, RPS24, DDX21, TEX10, WDR18, WDR3, CCT3, BMS1, GEMIN5, RPS14, RPS16, RPS18, RPS27, RPL13, RPL18, NOP56, EIF4A3	4.90E−06

[a]Selected proteins found to associate with Pf1 through LC-MS/MS analysis are shown. Genes are grouped according to their association with the indicated gene ontology biological process terms. The *P* values indicated were obtained using the DAVID functional annotation tool and the list of all proteins identified to be associated with wt Pf1 in our LC-MS/MS analysis.

protein Sin3A or Sin3B, depending on the experimental and/or cellular context. Biochemical studies have now revealed that Pf1 serves as an integral component of a small HDAC1/2-containing complex that comprises the Sin3B, HDAC1/2, and Mrg15 proteins (2–5). Pf1, like Sin3B, Mrg15, or HDAC1/2, is essential for embryonic development. However, the cellular phenotypes elicited upon Pf1 inactivation that we report here differed drastically from those resulting from the genetic deletion of Sin3B. Indeed, we have previously demonstrated that Sin3B inactivation in primary mouse embryonic fibroblasts does not impact cellular proliferation under normal culture conditions but impairs cell cycle exit triggered by proquiescence or prosenescence signals (10–12). In contrast, Pf1-null MEFs are unable to sustain proliferation, and they enter spontaneous premature senescence under normal culture conditions. The discrepancy between Pf1- and Sin3B-null MEF phenotypes may be attributed to the partial redundancy between Sin3B and its close paralog, Sin3A. Indeed, Sin3A inactivation is incompatible with cellular proliferation. While our previous report suggested that the interaction between Sin3B and Pf1 is tighter than the one between Sin3A and Pf1 (6), it is important to note that our proteomic study clearly identified Sin3A to be a Pf1 interactor. Interestingly, the phenotypes elicited upon Mrg15 inactivation are reminiscent of those uncovered in Pf1-null cells. Indeed, Tominaga and colleagues observed that Mrg15$^{-/-}$ embryos present growth retardation and delayed development of many organs and tissues, as well as defective cell proliferation and differentiation (17). Interestingly, Mrg15-null cells adopt senescent phenotypes prematurely and cease to proliferate earlier than their wild-type counterparts, a phenotype that is shared by Pf1-null MEFs. While Mrg15 is an integral part of two distinct chromatin-modifying complexes, the Sin3-Pf1-HDAC complex and the NuA4 complex, the phenotypes elicited upon Mrg15 inactivation are strikingly similar to those that we report here in Pf1-null embryos and cells. Thus, it is tempting to speculate that the resembling phenotypes elicited upon Mrg15 or Pf1 inactivation reflect the functional interaction between the two proteins. In that aspect, it is important to note that Eaf3, the yeast homolog of Mrg15, is dispensable for a functional NuA4 complex (34).

Cellular senescence is a stable cell cycle arrest in response to various cellular stresses (35–37). Many stimuli trigger senescence in primary cells. This includes oxidative stress, DNA damage, the expression of activated oncogenes (oncogene-induced senescence), or serial passaging, which drives the cell to replicative senescence (38). Thus, senescence is often seen as a mechanism to prevent damaged or mutated cells from proliferating uncontrollably (39). Interestingly, senescent cells often present morphological changes in the nucleolus, showing a single, very prominent nucleolus instead of a few smaller ones (20, 21). Our results indicate that Pf1 controls specific steps of ribosome biogenesis, such as splicing, covalent modifications, and maturation of the pre-rRNA transcripts, and that the changes observed in the nucleoli of Pf1$^{-/-}$ MEFs are unlikely to be an unspecific, secondary consequence of the changes in the rate at which the Pf1$^{-/-}$ cells proliferate. Interestingly, it was reported earlier that premature aging in yeast Werner helicase Sgs1 mutants correlates with alterations of the nucleolar

structure, reminiscent of what we observed in Pf1$^{-/-}$ MEFs (40). Given the functional link between senescence and aging in mammals (41), it is tempting to speculate that Pf1 engages a program that coordinates nucleolar integrity and prevention of premature aging. In that aspect, it is intriguing to note the recent demonstration that perturbation of ribosomal biogenesis results in the activation of a senescence program in mammalian cells (42).

It is also worth mentioning that the yeast Rpd3-Sin3 complex has been shown to catalyze histone H4 deacetylation at rDNA chromatin through this mechanism to control RNA polymerase I localization, rDNA transcription, and, as a consequence, the shape and size of the nucleolus in yeast cells (43). The results of experiments conducted in mammalian cells suggest that NoRC, an SNF2h-containing nucleolar chromatin remodeling complex, silences the rDNA locus by targeting the Sin3 corepressor complex to rDNA promoters (44). Given our observation that only the outer layers of the nucleolus are altered in Pf1$^{-/-}$ MEFs, it is unlikely that Pf1 alters ribosomal biogenesis directly through the modulation of rDNA transcription. Indeed, we were unable to detect an alteration in the amount of transcripts corresponding to rRNA in the absence of Pf1 (data not shown). Together, these observations point to a role of Pf1 in posttranscriptional events linked to ribosomal biogenesis.

Our coimmunoprecipitation experiments confirmed the interaction of Pf1 with PELP1, LAS1L, and NPM1. Previous studies showed that inactivation of these proteins can, directly or not, induce senescence, similar to what we observed during Pf1 inactivation. First, NPM1 was recently identified to control a p53-mediated cellular senescence. Using a model of colorectal cancer, Wong and colleagues showed that the suppression of NPM1 activity reduces viability and enhances senescence and cell cycle arrest (45). Second, PELP1 silencing was also shown to promote senescence and inhibit proliferation, colony formation, migration, invasion, and xenograft formation in the same colorectal cancer model (46). Finally, LAS1L inactivation has been showed to result in G_1 arrest, linking LAS1L to cell cycle progression (47). Moreover, SENP3, which we showed is more abundant in the Pf1$^{-/-}$ MEFs than in the control cells, interacts with NPM1 (26, 27, 30) and forms a nucleolar complex with PELP1 and LAS1L (47). If the results of our experiments cannot completely rule out the possibility of an indirect role of Pf1 in ribosomal biogenesis, the results of our LC-MS/MS and subsequent co-IP analyses suggest that the effect of Pf1 on nucleolar functions might not be mediated or at least might not be mediated solely by the Pf1 association with the Sin3-MRG15-HDAC complex. It will therefore be particularly important to perform an exhaustive characterization of the different protein complexes in which Pf1 is present, in order to understand how Pf1 executes its function in ribosome biogenesis and to discriminate between this function in ribosome biogenesis from the one that has already been characterized to be a transcriptional regulator. Indeed, we have previously shown that the Pf1 complex modulates RNAPII-driven transcription. In that aspect, it is important to note that recent findings have demonstrated that specific factors can coordinate the transcriptional regulation of ribosomal proteins and rRNA maturation (48). Our results suggest that Pf1 and its associated chromatin-modifying activities may also coordinate several steps in the generation of functional ribosomal subunits.

In conclusion, the results of our study point to a central function for a chromatin-associated protein in the regulation of ribosomal biogenesis and senescence. Whether this property of Pf1 contributes to the alteration of nucleolar functions and the accumulation of senescent cells in physiological settings, such as replicative aging or the response to exogenous stress, remains to be investigated.

MATERIALS AND METHODS

Generation of a Pf1 knockout mouse line. Pf1$^{-/-}$ mice were derived using the gene-trapping technique. Briefly, this included the identification of an embryonic stem (ES) cell clone with a ROSA26geo cassette integrated into the intron between exons 2 and 3 of the *Pf1* locus, subsequent microinjection of the selected ES cells into blastocysts to generate chimeric mice, and derivation of Pf1$^{+/-}$ mice. The

heterozygous animals were intercrossed, and embryos were collected at different time points. All procedures involving the use of animal experimentation were approved by the New York University (NYU) IACUC and Institutional Biosafety Committee (IBC).

Histology and IHC. Mouse embryos were fixed overnight in 10% formalin (Thermo Fisher Scientific, Waltham, MA) and processed for paraffin embedding. For histology, deparaffinized sections (5 μm) were stained with Gill's hematoxylin (Richard-Allan Scientific) and eosin Y, followed by an alcohol dehydration series and mounting (Permount; Thermo Fisher Scientific, Waltham, MA). Trichrome staining was performed at the NYU School of Medicine Histopathology Core Facility. Paraformaldehyde-fixed, paraffin-embedded, 4-μm sections of tissue were stained using unconjugated polyclonal rabbit anti-mouse cleaved caspase-3 (Asp-175) (catalog number 9661S; lot number 42 RRID:AB_331440; Cell Signaling Technology) and unconjugated rabbit anti-mouse Ki67 clone SP7 (catalog number RM-9106; lot number 1308g RRID:AB_2335745; Lab Vision).

MEF isolation, cells, and reagents. Mouse embryonic fibroblasts (MEFs) were generated from embryos at 13.5 and 14.5 days postcoitus. The head and the red organs were removed and used for genotyping. The torso was then minced and dispersed in 0.1% trypsin (45 min at 37°C). Cells were subsequently grown in Dulbecco modified Eagle medium (DMEM) supplemented with 10% fetal bovine serum (FBS; Atlanta Biologicals, Flowery Branch, GA), 50 μM β-mercaptoethanol (Sigma-Aldrich, St. Louis, MO), and penicillin-streptomycin and subcultured 1:4 upon confluence. The cultures were maintained in 6% O_2, 5% CO_2 at 37°C.

The HeLa S3 cell line was maintained in serum-like modified Eagle medium supplemented with 10% fetal bovine serum, 2 mM glutamine (Corning Inc., Corning, NY), and 1% nonessential amino acids (NEAA; Corning Inc., Corning, NY). The cultures were maintained in spinner flasks at 3×10^5 to 9×10^5 cells/ml in 5% CO_2 at 37°C.

293T cells were cultured in DMEM supplemented with 10% donor calf serum (DCS; Atlanta Biologicals, Flowery Branch, GA) and penicillin-streptomycin (Corning Inc., Corning, NY) and subcultured 1:4 upon confluence. The cultures were maintained in 5% CO_2 at 37°C. 293T cells were transfected using a standard calcium phosphate transfection protocol. The viral particles produced were collected for three consecutive days as a suspension in cell culture medium. The virus suspension supplemented with 6 μg/ml Polybrene (Millipore-Merck KGaA, Darmstadt, Germany) was filtered through a Millex-HV syringe filter unit (pore size, 0.45 μm; Millipore-Merck KGaA, Darmstadt, Germany) and used to infect the HeLa S3 cells.

3T3 protocol and growth curve. Growth curve experiments were performed essentially as described previously (49). Briefly, 25,000 cells per well were plated into 12-well plates. At the times indicated above, cells were washed with phosphate-buffered saline (PBS), fixed in 10% formalin, and rinsed with distilled water. Cells were stained with 0.1% crystal violet (Sigma-Aldrich, St. Louis, MO) for 30 min, rinsed extensively, and dried. Cell-associated dye was extracted with 2.0 ml 10% acetic acid. Aliquots were diluted 1:4 with H_2O and transferred to 96-well microtiter plates, and the optical density at 590 nm was determined. Values were normalized to the optical density at day 0 for the appropriate cell type. Within an experiment, each point was determined in triplicate; each growth curve was performed at least twice.

Gene expression microarray analysis and qPCR. Total RNA was isolated from $Pf1^{+/+}$ and $Pf1^{-/-}$ MEFs at passage 2 or 3 ($Pf1^{+/+}$ lines 7706-5 and 7706-6 and $Pf1^{-/-}$ lines 7706-2 and 7706-4) using the TRIzol reagent (Thermo Fisher Scientific, Waltham, MA) according to the manufacturer's protocol. The RNA samples were examined on an Affymetrix GeneChip mouse genome 430A (version 2.0) array (Affymetrix, Santa Clara, CA). Data were analyzed using GenePattern software (50) and Database for Annotation, Visualization, and Integrated Discovery (DAVID) tools (51, 52). cDNA was synthesized using Moloney murine leukemia virus reverse transcriptase (M-MLV RT; Promega, Madison, WI), and quantitative RT-PCR analyses were performed using Maxima SYBR green–carboxy-X-rhodamine 2× quantitative PCR (qPCR) master mix (Thermo Fisher Scientific, Waltham, MA), by following optimized manufacturer protocols.

BrdU incorporation. Subconfluent cultures were labeled for 2 h with 30 μM BrdU (Amersham). Cells were detached with trypsin, fixed in 4% paraformaldehyde, treated with 4 N HCl for 10 min at room temperature and 0.1 M borate (pH 8.5) for 2 min at room temperature (with PBS washes between each step), and, finally, permeabilized with 0.1% Triton X-100–3% bovine serum albumin (BSA)–PBS-Tween 20 (PBS-T) for 5 min. After subsequent washing steps in PBS-T, the cells were then incubated with BrdU antibody (dilution, 1:100 in PBS-T) for 80 min and then with a fluorescein isothiocyanate (FITC)-conjugated secondary antibody (dilution, 1:500 in PBS-T; Calbiochem-Merck KGaA, Darmstadt, Germany). The cells were counterstained with DAPI (4′,6-diamidino-2-phenylindole) to identify all nuclei, and the percentage of BrdU-labeled cells (cells labeled with FITC and DAPI) was quantified using a fluorescence microscope. At least 200 cells were counted per sample; each experiment was performed at least three times.

SA-β-Gal assay. Cells were washed in PBS, fixed for 3 to 5 min (room temperature) in 3% formaldehyde, washed, and incubated at 37°C with fresh X-Gal (5-bromo-4-chloro-3-indolyl-β-D-galactopyranoside) solution, consisting of 1× citric buffer (25 mM Na_2HPO_4, 7.4 mM citric acid, pH 6.0), 150 mM NaCl, 2 mM $MgCl_2$, 5 mM potassium ferricyanide, 5 mM potassium ferrocyanide, and 1 mg/ml X-Gal. Cells were incubated at 37°C overnight. The percentage of SA-β-Gal-positive cells was quantified using a phase-contrast inverted microscope. At least 200 cells were counted per sample; each experiment was performed at least three times.

Immunofluorescence. Cells were grown on coverslips to subconfluence, washed with PBS, and fixed in 3% paraformaldehyde–PBS for 10 min at room temperature. Fixed cells were permeabilized with Triton

X-100 buffer (0.1% Triton X-100, 20 mM HEPES-KOH, pH 7.9, 50 mM NaCl, 3 mM $MgCl_2$, 300 mM sucrose) for 5 min and blocked in 0.5% (wt/vol) BSA (Thermo Fisher Scientific, Waltham, MA) in PBS for 30 min at room temperature. The cells were then incubated with primary antibody in 0.5% (wt/vol) BSA in PBS for 2 h at room temperature, followed by three 5-min washes with PBS. Fluorescently labeled secondary antibodies in PBS were then added for 1 h at room temperature, and coverslips were washed 3 times with PBS. The primary antibodies used were anti-γ-H2A.X (catalog no. 05-636; Upstate, Millipore-Merck KGaA, Darmstadt, Germany), antifibrillarin (catalog no. 2639S; Cell Signaling, Danvers, MA), anti-UBF (catalog no. sc-9131; Santa Cruz Biotechnology, Inc., Dallas, TX), and anti-SENP3 (catalog no. 5591S; Cell Signaling, Danvers, MA). The cells were counterstained with TO-PRO3 (Thermo Fisher Scientific, Waltham, MA) by following the manufacturer's protocol and visualized by confocal microscopy.

Coimmunoprecipitation and LC-MS/MS. Transfections and coimmunoprecipitations were performed essentially as described previously (6), using an EZview red anti-Flag M2 affinity gel (Sigma-Aldrich, St. Louis, MO) during the overnight incubation step. Constructs of Pf1 wt and mutant proteins were generated in the David lab. The tagged constructs of APC6, APC7, and APC8 used in the coimmunoprecipitation experiments were obtained from D. Izawa (Cambridge, UK). Plasmids expressing PELP1, LAS1L, and NPM1 were a gift from S. Muller (Frankfurt, Germany, and Cambridge, UK), and plasmids expressing Sec13 and NABP2 were obtained from M. Pagano (New York, NY). Pf1 immunoprecipitation samples were reduced, alkylated, and run into a gel to remove any detergents and other mass spectrometry-incompatible reagents. The gel plugs were excised, digested with trypsin in gel, extracted, and desalted (53). Following desalting, the peptide mixtures were gradient eluted directly into a Thermo Scientific Q Exactive mass spectrometer. Data were searched using the Sequest program within the Proteome Discoverer software suite for peptide and protein identifications.

Accession number(s). The raw data from the microarray experiment have been deposited in the GEO database with GEO accession number GSE86398.

ACKNOWLEDGMENTS

We thank the staff of NYU Langone School of Medicine, B. Ueberheide, and the Proteomics Resource Center for assistance with the proteomics experiments, A. Heguy and the Genome Technology Center for assistance with the microarray experiments, and Esthelle Hoedt for help with proteomics data analyses. We also thank Beatriz Fontoura, John Goodier, Daisuke Izawa, Stefan Muller, and Celine Verheggen for the generous gift of reagents.

The work reported here was supported by the National Institutes of Health (R01CA148639 and R21CA155736 to G.D.), the Samuel Waxman Cancer Research Foundation (to G.D.), and a Feinberg NYU individual grant (to G.D.). K.M. was supported by departmental training grant 5-T32CA9161-40. The mass spectrometric experiments were in part supported by Cancer Center support grant P30CA016087 at the Laura and Isaac Perlmutter Cancer Center. The Proteomics Resource Center and the Genome Technology Center are supported in part by NIH/NCI support grant P30CA016087.

REFERENCES

1. Musselman CA, Kutateladze TG. 2011. Handpicking epigenetic marks with PHD fingers. Nucleic Acids Res 39:9061–9071. https://doi.org/10.1093/nar/gkr613.
2. Yochum GS, Ayer DE. 2001. Pf1, a novel PHD zinc finger protein that links the TLE corepressor to the mSin3A-histone deacetylase complex. Mol Cell Biol 21:4110–4118. https://doi.org/10.1128/MCB.21.13.4110-4118.2001.
3. Hayakawa T, Ohtani Y, Hayakawa N, Shinmyozu K, Saito M, Ishikawa F, Nakayama J. 2007. RBP2 is an MRG15 complex component and down-regulates intragenic histone H3 lysine 4 methylation. Genes Cells 12:811–826.
4. Yochum GS, Ayer DE. 2002. Role for the mortality factors MORF4, MRGX, and MRG15 in transcriptional repression via associations with Pf1, mSin3A, and Transducin-Like Enhancer of Split. Mol Cell Biol 22:7868–7876. https://doi.org/10.1128/MCB.22.22.7868-7876.2002.
5. Xie T, Graveline R, Kumar GS, Zhang Y, Krishnan A, David G, Radhakrishnan I. 2012. Structural basis for molecular interactions involving MRG domains: implications in chromatin biology. Structure 20:151–160. https://doi.org/10.1016/j.str.2011.10.019.
6. Jelinic P, Pellegrino J, David G. 2011. A novel mammalian complex containing Sin3B mitigates histone acetylation and RNA polymerase II progression within transcribed loci. Mol Cell Biol 31:54–62. https://doi.org/10.1128/MCB.00840-10.
7. Kaadige MR, Ayer DE. 2006. The polybasic region that follows the plant homeodomain zinc finger 1 of Pf1 is necessary and sufficient for specific phosphoinositide binding. J Biol Chem 281:28831–28836. https://doi.org/10.1074/jbc.M605624200.
8. Strobl-Mazzulla PH, Bronner ME. 2012. A PHD12-Snail2 repressive complex epigenetically mediates neural crest epithelial-to-mesenchymal transition. J Cell Biol 198:999–1010. https://doi.org/10.1083/jcb.201203098.
9. Bansal N, Petrie K, Christova R, Chung CY, Leibovitch BA, Howell L, Gil V, Sbirkov Y, Lee E, Wexler J, Ariztia EV, Sharma R, Zhu J, Bernstein E, Zhou MM, Zelent A, Farias E, Waxman S. 2015. Targeting the SIN3A-PF1 interaction inhibits epithelial to mesenchymal transition and maintenance of a stem cell phenotype in triple negative breast cancer. Oncotarget 6:34087–34105. https://doi.org/10.18632/oncotarget.6048.
10. David G, Grandinetti KB, Finnerty PM, Simpson N, Chu GC, Depinho RA. 2008. Specific requirement of the chromatin modifier mSin3B in cell cycle exit and cellular differentiation. Proc Natl Acad Sci U S A 105:4168–4172. https://doi.org/10.1073/pnas.0710285105.
11. Grandinetti KB, David G. 2008. Sin3B: an essential regulator of chromatin modifications at E2F target promoters during cell cycle withdrawal. Cell Cycle 7:1550–1554. https://doi.org/10.4161/cc.7.11.6052.
12. Grandinetti KB, Jelinic P, DiMauro T, Pellegrino J, Fernandez Rodriguez R, Finnerty PM, Ruoff R, Bardeesy N, Logan SK, David G. 2009. Sin3B expression is required for cellular senescence and is up-regulated upon oncogenic stress. Cancer Res 69:6430–6437. https://doi.org/10.1158/0008-5472.CAN-09-0537.
13. Rielland M, Cantor DJ, Graveline R, Hajdu C, Mara L, Diaz BDD, Miller G,

David G. 2014. Senescence-associated SIN3B promotes inflammation and pancreatic cancer progression. J Clin Invest 124:2125–2135. https://doi.org/10.1172/JCI72619.
14. Lagger G, O'Carroll D, Rembold M, Khier H, Tischler J, Weitzer G, Schuettengruber B, Hauser C, Brunmeir R, Jenuwein T, Seiser C. 2002. Essential function of histone deacetylase 1 in proliferation control and CDK inhibitor repression. EMBO J 21:2672–2681. https://doi.org/10.1093/emboj/21.11.2672.
15. Montgomery RL, Davis CA, Potthoff MJ, Haberland M, Fielitz J, Qi X, Hill JA, Richardson JA, Olson EN. 2007. Histone deacetylases 1 and 2 redundantly regulate cardiac morphogenesis, growth, and contractility. Genes Dev 21:1790–1802. https://doi.org/10.1101/gad.1563807.
16. Wilting RH, Yanover E, Heideman MR, Jacobs H, Horner J, van der Torre J, DePinho RA, Dannenberg JH. 2010. Overlapping functions of Hdac1 and Hdac2 in cell cycle regulation and haematopoiesis. EMBO J 29:2586–2597. https://doi.org/10.1038/emboj.2010.136.
17. Tominaga K, Kirtane B, Jackson JG, Ikeno Y, Ikeda T, Hawks C, Smith JR, Matzuk MM, Pereira-Smith OM. 2005. MRG15 regulates embryonic development and cell proliferation. Mol Cell Biol 25:2924–2937. https://doi.org/10.1128/MCB.25.8.2924-2937.2005.
18. Di Micco R, Sulli G, Dobreva M, Liontos M, Botrugno OA, Gargiulo G, dal Zuffo R, Matti V, d'Ario G, Montani E, Mercurio C, Hahn WC, Gorgoulis V, Minucci S, d'Adda di Fagagna F. 2011. Interplay between oncogene-induced DNA damage response and heterochromatin in senescence and cancer. Nat Cell Biol 13:292–302. https://doi.org/10.1038/ncb2170.
19. Boisvert FM, van Koningsbruggen S, Navascues J, Lamond AI. 2007. The multifunctional nucleolus. Nat Rev Mol Cell Biol 8:574–585.
20. Holmberg Olausson K, Nister M, Lindstrom MS. 2012. p53-dependent and -independent nucleolar stress responses. Cells 1:774–798. https://doi.org/10.3390/cells1040774.
21. Kar B, Liu B, Zhou Z, Lam YW. 2011. Quantitative nucleolar proteomics reveals nuclear re-organization during stress-induced senescence in mouse fibroblast. BMC Cell Biol 12:33. https://doi.org/10.1186/1471-2121-12-33.
22. Sobol M, Yildirim S, Philimonenko VV, Marasek P, Castano E, Hozak P. 2013. UBF complexes with phosphatidylinositol 4,5-bisphosphate in nucleolar organizer regions regardless of ongoing RNA polymerase I activity. Nucleus 4:478–486. https://doi.org/10.4161/nucl.27154.
23. Newton K, Petfalski E, Tollervey D, Caceres JF. 2003. Fibrillarin is essential for early development and required for accumulation of an intron-encoded small nucleolar RNA in the mouse. Mol Cell Biol 23:8519–8527. https://doi.org/10.1128/MCB.23.23.8519-8527.2003.
24. Adams PD. 2007. Remodeling of chromatin structure in senescent cells and its potential impact on tumor suppression and aging. Gene 397:84–93. https://doi.org/10.1016/j.gene.2007.04.020.
25. Tollervey D, Lehtonen H, Jansen R, Kern H, Hurt EC. 1993. Temperature-sensitive mutations demonstrate roles for yeast fibrillarin in pre-rRNA processing, pre-rRNA methylation, and ribosome assembly. Cell 72:443–457. https://doi.org/10.1016/0092-8674(93)90120-F.
26. Finkbeiner E, Haindl M, Raman N, Muller S. 2011. SUMO routes ribosome maturation. Nucleus 2:527–532. https://doi.org/10.4161/nucl.2.6.17604.
27. Finkbeiner E, Haindl M, Muller S. 2011. The SUMO system controls nucleolar partitioning of a novel mammalian ribosome biogenesis complex. EMBO J 30:1067–1078. https://doi.org/10.1038/emboj.2011.33.
28. Grisendi S, Mecucci C, Falini B, Pandolfi PP. 2006. Nucleophosmin and cancer. Nat Rev Cancer 6:493–505. https://doi.org/10.1038/nrc1885.
29. Haindl M, Harasim T, Eick D, Muller S. 2008. The nucleolar SUMO-specific protease SENP3 reverses SUMO modification of nucleophosmin and is required for rRNA processing. EMBO Rep 9:273–279. https://doi.org/10.1038/embor.2008.3.
30. Raman N, Nayak A, Muller S. 2014. mTOR signaling regulates nucleolar targeting of the SUMO-specific isopeptidase SENP3. Mol Cell Biol 34:4474–4484. https://doi.org/10.1128/MCB.00801-14.
31. Kumar GS, Chang W, Xie T, Patel A, Zhang Y, Wang GG, David G, Radhakrishnan I. 2012. Sequence requirements for combinatorial recognition of histone H3 by the MRG15 and Pf1 subunits of the Rpd3S/Sin3S corepressor complex. J Mol Biol 422:519–531. https://doi.org/10.1016/j.jmb.2012.06.013.
32. Benevolenskaya EV, Murray HL, Branton P, Young RA, Kaelin WG, Jr. 2005. Binding of pRB to the PHD protein RBP2 promotes cellular differentiation. Mol Cell 18:623–635. https://doi.org/10.1016/j.molcel.2005.05.012.
33. Florens L, Carozza MJ, Swanson SK, Fournier M, Coleman MK, Workman JL, Washburn MP. 2006. Analyzing chromatin remodeling complexes using shotgun proteomics and normalized spectral abundance factors. Methods 40:303–311. https://doi.org/10.1016/j.ymeth.2006.07.028.
34. Mitchell L, Lambert JP, Gerdes M, Al-Madhoun AS, Skerjanc IS, Figeys D, Baetz K. 2008. Functional dissection of the NuA4 histone acetyltransferase reveals its role as a genetic hub and that Eaf1 is essential for complex integrity. Mol Cell Biol 28:2244–2256. https://doi.org/10.1128/MCB.01653-07.
35. Collado M. 2010. Exploring a 'pro-senescence' approach for prostate cancer therapy by targeting PTEN. Future Oncol 6:687–689. https://doi.org/10.2217/fon.10.39.
36. Collado M, Serrano M. 2010. Senescence in tumours: evidence from mice and humans. Nat Rev Cancer 10:51–57. https://doi.org/10.1038/nrc2772.
37. Sharpless NE, Sherr CJ. 2015. Forging a signature of in vivo senescence. Nat Rev Cancer 15:397–408. https://doi.org/10.1038/nrc3960.
38. Dimauro T, David G. 2009. Chromatin modifications: the driving force of senescence and aging? Aging (Albany NY) 1:182–190.
39. Kuilman T, Michaloglou C, Mooi WJ, Peeper DS. 2010. The essence of senescence. Genes Dev 24:2463–2479. https://doi.org/10.1101/gad.1971610.
40. Sinclair DA, Mills K, Guarente L. 1997. Accelerated aging and nucleolar fragmentation in yeast sgs1 mutants. Science 277:1313–1316. https://doi.org/10.1126/science.277.5330.1313.
41. van Deursen JM. 2014. The role of senescent cells in ageing. Nature 509:439–446. https://doi.org/10.1038/nature13193.
42. Nishimura K, Kumazawa T, Kuroda T, Katagiri N, Tsuchiya M, Goto N, Furumai R, Murayama A, Yanagisawa J, Kimura K. 2015. Perturbation of ribosome biogenesis drives cells into senescence through 5S RNP-mediated p53 activation. Cell Rep 10:1310–1323. https://doi.org/10.1016/j.celrep.2015.01.055.
43. Tsang CK, Bertram PG, Ai W, Drenan R, Zheng XF. 2003. Chromatin-mediated regulation of nucleolar structure and RNA Pol I localization by TOR. EMBO J 22:6045–6056. https://doi.org/10.1093/emboj/cdg578.
44. Zhou Y, Santoro R, Grummt I. 2002. The chromatin remodeling complex NoRC targets HDAC1 to the ribosomal gene promoter and represses RNA polymerase I transcription. EMBO J 21:4632–4640. https://doi.org/10.1093/emboj/cdf460.
45. Wong JC, Hasan MR, Rahman M, Yu AC, Chan SK, Schaeffer DF, Kennecke HF, Lim HJ, Owen D, Tai IT. 2013. Nucleophosmin 1, upregulated in adenomas and cancers of the colon, inhibits p53-mediated cellular senescence. Int J Cancer 133:1567–1577. https://doi.org/10.1002/ijc.28180.
46. Ning Z, Zhang Y, Chen H, Wu J, Song T, Wu Q, Liu F. 2014. PELP1 suppression inhibits colorectal cancer through c-Src downregulation. Oxid Med Cell Longev 2014:193523. https://doi.org/10.1155/2014/193523.
47. Castle CD, Cassimere EK, Denicourt C. 2012. LAS1L interacts with the mammalian Rix1 complex to regulate ribosome biogenesis. Mol Biol Cell 23:716–728. https://doi.org/10.1091/mbc.E11-06-0530.
48. Calo E, Flynn RA, Martin L, Spitale RC, Chang HY, Wysocka J. 2015. RNA helicase DDX21 coordinates transcription and ribosomal RNA processing. Nature 518:249–253. https://doi.org/10.1038/nature13923.
49. Serrano M, Lin AW, McCurrach ME, Beach D, Lowe SW. 1997. Oncogenic ras provokes premature cell senescence associated with accumulation of p53 and p16INK4a. Cell 88:593–602. https://doi.org/10.1016/S0092-8674(00)81902-9.
50. Reich M, Liefeld T, Gould J, Lerner J, Tamayo P, Mesirov JP. 2006. GenePattern 2.0. Nat Genet 38:500–501. https://doi.org/10.1038/ng0506-500.
51. Huang DW, Sherman BT, Lempicki RA. 2009. Systematic and integrative analysis of large gene lists using DAVID bioinformatics resources. Nat Protoc 4:44–57. https://doi.org/10.1038/nprot.2008.211.
52. Huang DW, Sherman BT, Zheng X, Yang J, Imamichi T, Stephens R, Lempicki RA. 2009. Extracting biological meaning from large gene lists with DAVID. Curr Protoc Bioinformatics 27:13.11.1–13.11.13. https://doi.org/10.1002/0471250953.bi1311s27.
53. Cotto-Rios XM, Bekes M, Chapman J, Ueberheide B, Huang TT. 2012. Deubiquitinases as a signaling target of oxidative stress. Cell Rep 2:1475–1484. https://doi.org/10.1016/j.celrep.2012.11.011.